Part Three

Multi-Dimensional Imaging and Display

11

Three-Dimensional Integral Imaging and Display

Manuel Martínez-Corral[1], Adrián Dorado[1], Anabel LLavador[1], Genaro Saavedra[1] and Bahram Javidi[2]

[1]*Department of Optics, University of Valencia, Spain*
[2]*Department of Electrical and Computer Engineering, University of Connecticut, USA*

11.1 Introduction

Conventional photographic cameras do not have the capacity to record all of the information carried by the rays of light passing through their objective lens, which indeed impacts on the image sensor pixels from many directions [1]. The irradiance collected by any pixel is proportional to the sum of radiances of all rays, regardless of their incidence angles. Thus, a typical picture obtained with a conventional camera contains, of course, a 2D image (or in other words a pixelated 2D irradiance map) of the original 3D object, in which any information about intensity and angle of impinging light rays is lost.

Much more interesting would be to have a system with the capacity of registering a map with the radiance and direction of all the rays proceeding from the 3D scene. Such a map has been named in different ways, such as integral photography, integral imaging, lightfield map, or even a *plenoptic* map.

Interest in the capture and display of 3D images is not a modern issue. In fact in 1838, Wheatstone [2] tackled the problem of displaying 3D images through the first stereoscope. Soon later, Rollman faced the same problem, but proposed the use of anaglyphs [3]. But the main problem of these techniques, and also of all the stereoscopic techniques developed since then, is that they do not actually produce a 3D reconstruction of a 3D scene. Instead, they produce a stereoscopic pair of images which, when projected onto the retinas of the left and right eyes, provides the brain with the sensation of perspective vision and depth discrimination. Apart from the problem that stereoscopy provides the same perspective to different observers, whatever their relative position to the screen, the main drawback comes from the conflict between

Multi-dimensional Imaging, First Edition. Edited by Bahram Javidi, Enrique Tajahuerce and Pedro Andrés.

convergence and accommodation [4]. This conflict occurs when the accommodation of the eye lens is fixed to one distance, whereas the convergence of the eyes' axes is set to a different distance. This is a strongly unnatural physiological procedure that gives rise to visual discomfort after prolonged observations.

The first scientist to propose a method for displaying/observing 3D images without the need for any special glasses was Gabriel Lippmann, who proposed the integral photography (IP) in 1908 [5–7]. Lippmann's idea was that it is possible to record the information of a 3D scene with a 2D sensor, provided that many perspectives of the scene are stored. To do that, Lippmann proposed to remove the objective from the camera and, instead, to insert a microlens array (MLA) in front of the sensor. This way of proceeding permits to record an integral image (InI), that is, a collection of elemental images each with a different perspective of the scene. The InI captured following Lippmann's recipe can be used for many proposals. One is for the implementation of an IP digital monitor [8–10]. For this task it is necessary to project the set of elemental images onto a pixelated display, like a LCD or LED monitor, and insert a MLA, similar to the one used in the capture, just in front. In the display process, any pixel of the LCD panel emits a light cone, which after passing through the corresponding microlens produces a light cylinder in free space. It is the intersection of all the ray cylinders that produces an irradiance distribution in front of the monitor, which reproduces the irradiance of the original 3D scene. This distribution is perceived as 3D by the observer, whatever his/her position, with a continuous viewpoint and also with full parallax. Since the observer is watching a real light concentration, the observation is produced without conflict between convergence and accommodation.

IP, like holography, is usually catalogued as an auto-stereoscopic technique due to the fact that it does not need the use of special glasses. However, auto-stereoscopic is a misleading name since it implies IP is based in stereoscopy, which is clearly not the case.

An alternative architecture for the capture of the integral image was proposed by Davies and McCormick [11], and later by Adelson and Wang [12]. The technique consisted of inserting a microlens array at the back-focal plane of a conventional photographic camera, in front of the sensor. Proceeding in this way, it is possible to capture the radiance map (or plenoptic picture) of far 3D scenes. This alternative architecture has been named as plenoptic camera [1,13,14], lightfield camera [14,15] and also far-field IP camera [16,17].

The IP concept was initially intended for the capture and display of 3D pictures or movies. In this sense, many important advances have been achieved in the search for the improvement of display resolution [18–22], viewing angle [23–25], or the depth of field [26–29]. However in the past few years, the computational reconstruction of the irradiance distribution of incoherent 3D scenes has become a major application [30–36]. This reconstruction can be very useful for depth segmentation of 3D objects [37–40], or for the sensing and recognition of 3D objects in normal [41–44] or in low light levels [45,46]. Other interesting applications of the IP concept are, for example, the tracking of moving objects in a 3D environment [47,48], the polarimetric discrimination [49], the integration of 3D hyperspectral information [50], the 3D microscopy [51–53], or even wavefront sensing [54].

The aim of this chapter is to expose in a simple manner the theory behind the IP concept, the relation between the different forms of capturing the radiance map, and the algorithms and methods for 3D depth reconstruction in the display of 3D scenes. To this end we have divided the chapter into eight sections. In Section 11.2 we expose the basic theory of conventional 2D image capturing. In Section 11.3 we define the plenoptic function and corresponding

transformation rules. In Section 11.4 we describe the different methods for capturing the plenoptic map. In Section 11.5 we study the transformations suffered by the plenoptic map when changing the reference plane, and also calculate the 2D picture associated to any plane. In Section 11.6 we calculate the reconstructed 3D scene for different methods of plenoptic map capture. In Section 11.7 we tackle the implementation of 3D IP displays. Finally, in Section 11.8 we summarize the main outcomes of this chapter.

11.2 Basic Theory

A diffusing or self-luminous object can be treated as a continuous distribution of point sources that emit light isotropically. Although the natural way of describing this emission is through the concept of a spherical wavefront, in what follows we will assume that the phenomena we deal with are well described by the ray-optics theory, in which rays are the carriers of light energy and propagate in a straight line. We also assume that the point sources are mutually incoherent so that light emitted by them cannot interfere.

The most common device for capturing light emitted by a 3D scene is the photographic camera. As shown in Fig. 11.1, to obtain a picture of a 3D scene the camera is set so that the sensor is conjugate with a plane of the object space, the *reference plane*. The light emitted by points on such a plane is registered sharply in the pixelated sensor. The sensor also records the light emitted by out-of-focus points but with some blurring, which depends on the geometrical parameters of the capture system. Since the behavior of the electronic sensor is, in good approximation, linear, any pixel register the sum of the radiances of all the rays impacting the pixel. Thus, the recorded picture contains the sharp image of the parts of the scene that are on the reference plane, plus blurred information from the rest of the scene. However, it does not contain any individualized information about the radiance of the rays that reach the pixels. The loss of this angular information prevents the recorded picture from recovering the 3D structure of the scene from a conventional picture.

The magnitude that allows an accurate description of angular and spatial information of propagated rays is the radiance, defined as the radiant flux, Φ, per unit of area, A, and unit of

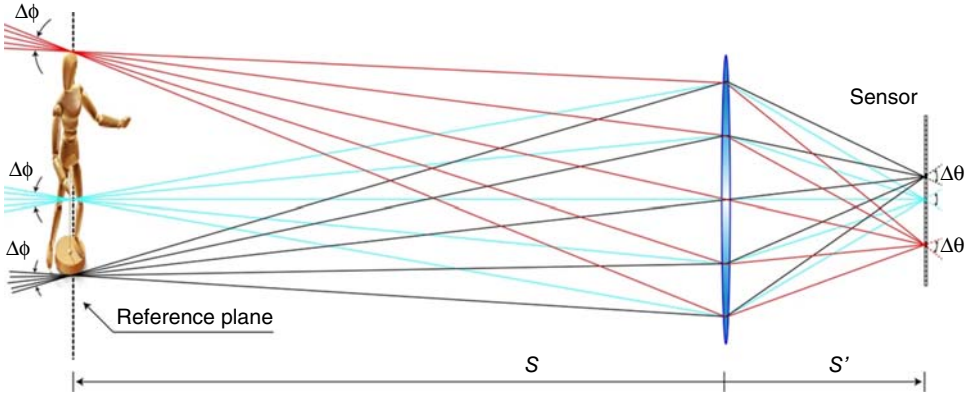

Figure 11.1 Optical scheme of a conventional photographic camera

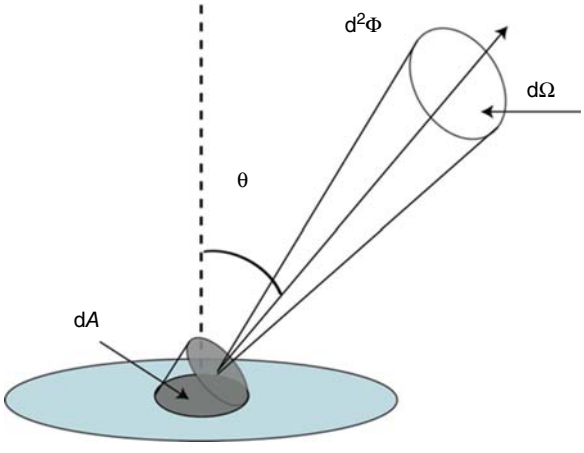

Figure 11.2 Scheme for the definition of the radiance

solid angle, emitted by a differential surface in a given direction. In mathematical terms the radiance

$$L = \frac{d^2\Phi}{d\Omega\, dA\, \cos\theta}, \tag{11.1}$$

where θ is the angle between the normal to the surface and the specified direction. This definition permits to establish the concept of ray of light as the light cone delimited by an infinitesimal solid angle, $d\Omega$, see Fig. 11.2. The 3D spatial distribution of radiance emitted by a 3D scene is usually named the *lightfield* or equivalently, the *plenoptic field*.

A ray of light can be parameterized through the spatial coordinates $\mathbf{r} = (x, y, z)$ of one point of its trajectory, and the angular coordinates $\boldsymbol{\theta} = (\theta, \phi)$ that describe its inclination. Then, given a region in the space, the plenoptic field is described by a 5D function. If we consider the case in which the rays propagate in a region free of occlusions and diffusing media, the direction and radiance of rays do not change with propagation. This redundancy permits saving one dimension in the description of the plenoptic field, and then parameterizing it through a 4D function. Following the paper by Georgiev and Lumsdaine [13] we can represent the plenoptic function as $L(\mathbf{x}, \boldsymbol{\theta})$, where $\mathbf{x} = (x, y)$. However, and for the sake of the simplicity in the forthcoming graphic representations, we will consider the case in which the plenoptic function is 2D, $L(x, \theta)$, so that we only will consider rays propagating on a plane. Naturally, this simplification does not subtract any generality to the forthcoming study.

11.3 The Plenoptic Function

The simplest example of the plenoptic field is that generated by a monochromatic point source. To build the 4D plenoptic function, first one has to select the plenoptic reference plane. This plane is typically perpendicular to the chief direction of propagation of the light beam. Then, one has to evaluate the inclination of rays when impacting the plenoptic reference plane. Assuming that the point source radiates isotropically, the plenoptic field at a plane placed at a distance z_0 from the source, is represented with a straight line, of slope $\mu = 1/z_0$, since there

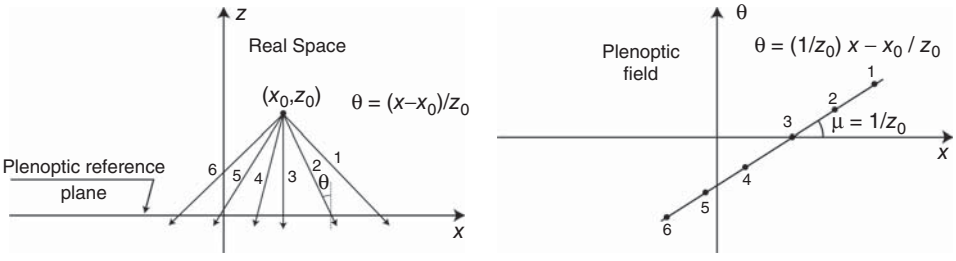

Figure 11.3 Plenoptic field generated by a monochromatic point source

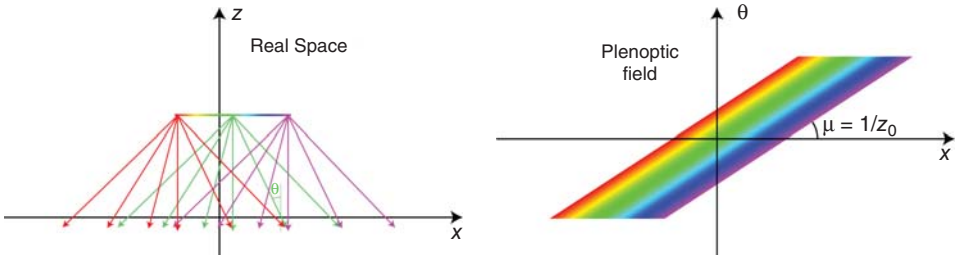

Figure 11.4 Plenoptic field generated by a monochromatic plane source

is direct proportionality (within the paraxial approximation) between the spatial coordinate of the impact point and the inclination angle (see Fig. 11.3).

Of similar complexity is the plenoptic field produced by a plane object that is set parallel to the plenoptic reference plane. Any point of the object is represented in the plenoptic diagram by a straight line. The bundle composed by the inclined lines produced by all the points of the plane object constitutes the plenoptic field, as shown in the Fig. 11.4.

It is interesting to find out how the plenoptic function changes when light propagates in free space, or when it passes through a converging lens. These transformations can be formalized by means of a transfer matrix [55]. The propagation in free space implies a change in the spatial coordinates, but not in the inclination angles, as shown in Fig. 11.5(a). The transfer matrix is of the form

$$T = \begin{pmatrix} 1 & t \\ 0 & 1 \end{pmatrix}, \tag{11.2}$$

where t is the propagation distance. The propagated plenoptic field can be obtained from the original one through the coordinates' transformation

$$\begin{pmatrix} x' \\ \theta' \end{pmatrix} = \begin{pmatrix} 1 & t \\ 0 & 1 \end{pmatrix} \begin{pmatrix} x \\ \theta \end{pmatrix} = \begin{pmatrix} x + t\theta \\ \theta \end{pmatrix}. \tag{11.3}$$

This can be understood as a shearing of the plenoptic function in the direction of the spatial coordinates, as shown in Fig.11.6(a).

Another interesting issue is to find out how the plenoptic field is modified when passing through a converging lens. As shown in Fig. 11.5(b), this transition implies a change in the

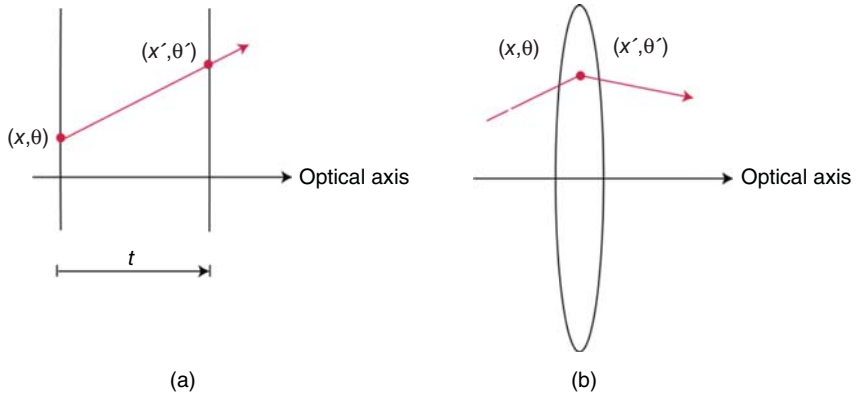

Figure 11.5 Coordinate transformation associated with (a) free space propagation and (b) refraction in a lens

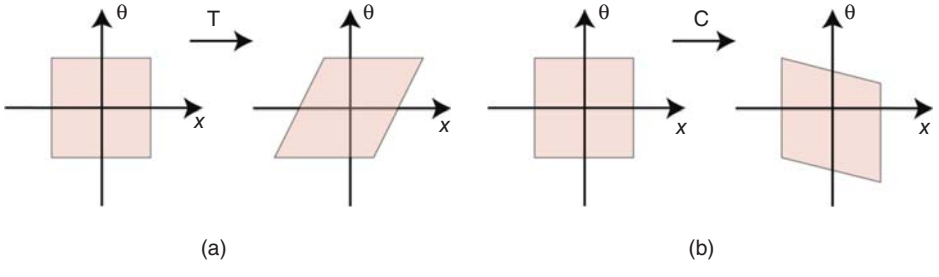

Figure 11.6 Shearing of the plenoptic function as result of (a) free-space propagation and (b) refraction in a lens

inclination angle of impinging rays, but not in the spatial coordinate. According to [55], the transfer matrix is

$$C = \begin{pmatrix} 1 & 0 \\ -1/f & 1 \end{pmatrix}, \tag{11.4}$$

where f is the focal length of the lens. The plenoptic field after refraction through the lens can be obtained from the impinging one by

$$\begin{pmatrix} x' \\ \theta' \end{pmatrix} = \begin{pmatrix} 1 & 0 \\ -1/f & 1 \end{pmatrix} \begin{pmatrix} x \\ \theta \end{pmatrix} = \begin{pmatrix} x \\ -x/f + \theta \end{pmatrix}. \tag{11.5}$$

Also in this case the plenoptic function suffers a shearing, but now in the angular direction, as shown in Fig. 11.6(b).

Let us remark that, from the plenoptic function evaluated in a plane, it is possible to calculate the "picture" by simply summing up the radiances at any point of that plane. In mathematical terms this can be made by calculation of the Abel transform [56] (or angular projection onto

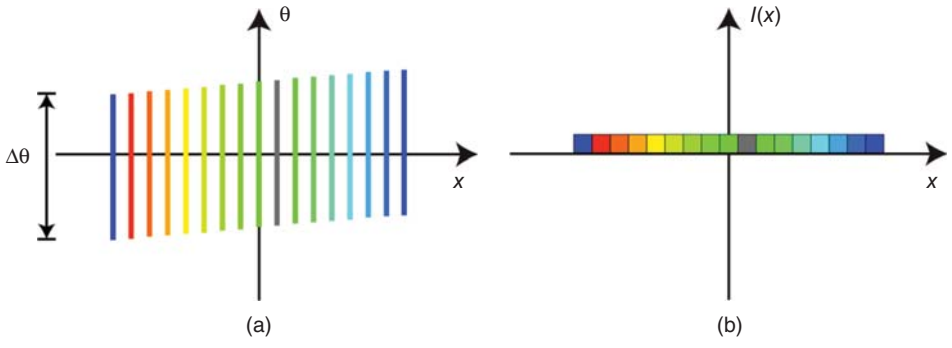

Figure 11.7 (a) Plenoptic filed captured by a conventional photographic camera; (b) registered picture, which is obtained as the angular projection of the plenoptic field

the spatial axis) of the plenoptic function; that is

$$I(\mathbf{x}) = \int L(\mathbf{x}, \boldsymbol{\theta}) d\boldsymbol{\theta}. \tag{11.6}$$

When a conventional photographic camera is used to record the light emitted by a 3D scene, any pixel captures all the rays passing through its conjugate in the object's reference plane (see Fig. 11.1). Expressed in terms of the plenoptic field, any pixel captures the plenoptic field contained in a vertical segment whose length is equal to the angle subtended by the aperture of the camera lens; see Fig. 11.7. Of course, the recorded picture is given by the Abel transform of the plenoptic function. It is apparent that, in the photographic shot, the angular information, and therefore the 3D information, is lost.

11.4 Methods for the Capture of the Plenoptic Field

11.4.1 Integral Photography

A very clever way of recording sampled information of the plenoptic field produced by 3D objects is the use of multiview camera systems. Such kind of systems can be implemented, as proposed by Lippmann [5], by placing a *microlens array* (MLA) in front of a light sensor. Other ways of implementing the IP capturing system, mainly useful when aiming the recording of the plenoptic field produced by large 3D scenes, is to use a set of digital cameras arranged in a rectangular grid. The picture captured by any camera is named here as an elemental image. As shown in Fig. 11.8, an array of equidistant cameras placed at the plenoptic reference plane can acquire sampled information of the plenoptic field. Any elemental image contains discrete information about the angles of rays passing through the center of the entrance pupil of the camera. Thus, every elemental image contains sampled information of a vertical line in the plenoptic function (see the black envelope in Fig. 11.8b). On the contrary, a horizontal line in the plenoptic diagram corresponds to a set of rays passing through the reference plane, equidistant and parallel to each other (see the white envelope in Fig. 11.8b). The pixels of a horizontal line can be grouped to form a sub-image of the 3D scene. These sub-images, which will be named *micro-images* here, are orthographic views of the 3D scene. Orthographic means

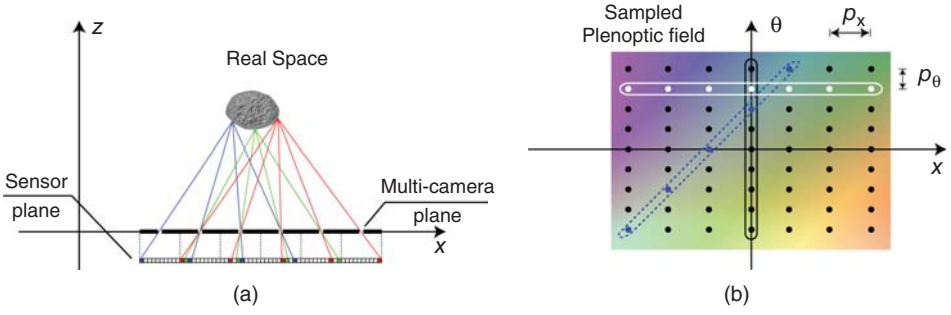

Figure 11.8 (a) Capture of the plenoptic field with a multi-camera system; (b) registered plenoptic field

Figure 11.9 Experimental set up for the acquisition of the elemental images

that the scale of the image does not depend on the distance from the object to the lens. Finally, an inclined line (see the dotted envelope) corresponds to the plenoptic field radiated by a point of the 3D scene.

Next, we describe a typical experiment for the capture of the plenoptic field with an experimental setup based on the IP concept (see Fig. 11.9). Although there are already some compact realizations of IP capturing setups [57,58], we used the so-called synthetic aperture method [59], in which all the elemental images are picked up with just one digital camera that is mechanically translated. The synchronized positioning, shooting, and recording of the elemental images was controlled by a LabVIEW® code. The digital camera (Canon 450D) was focused at the wooden panel, which was placed at a distance of 630 *mm*. The camera parameters were fixed to $f = 18$ mm and $f_\# = 22.0$, so that the depth of field was large enough obtain sharp pictures of the entire 3D scene. With the setup there is a set of $N_H = N_V = 11$ elemental images with pitch $P_H = P_V = 10.0$ mm. Since the pitch is smaller than the size of the CCD sensor (22.2 × 14.8 mm), we cropped every elemental image to remove the outer parts. In

Figure 11.10 Subset of the elemental images obtained experimentally

addition, we resized the elemental images so that any image was composed by $n_H = n_V = 300$ pixels.

Next, in Fig. 11.10 we show a subset ($N_H = 11$ and $N_V = 5$) of the captured elemental images. Note that each elemental image stores different perspective information about the 3D scene. From the elemental image set (the InI) one can easily calculate the micro-images by simply extracting and composing the pixels with the same local position in every elemental image. This transposition of the plenoptic information allowed for calculation of $N_H = 300 \times N_V = 300$ micro-images composed each by $n_H = 11 \times n_V = 11$ pixels. In the Fig. 11.11 we show the complete micro-image collection.

11.4.2 The Plenoptic Camera

Based on the concepts reported by Lippmann, some research groups (Davies and McCormick [11], Adelson and Wang [12], and later Okano *et al*. [17]) proposed a technique for recording, after a single snapshot, the radiance emitted by a 3D scene. Due to Adelson and Wang, this setup is known as the *plenoptic camera*.

A scheme of this camera is shown in Fig. 11.12. In the plenoptic camera an array of microlenses is inserted in front of the sensor. This new architecture, in which the 3D scene is not directly in front of the MLA but projected close to it, is useful in the case of far objects, or for special applications like microphotography or ophthalmoscopy. The conjugation relations are of great importance in the plenoptic scheme. Specifically, the system is adjusted in such a way that the reference plane is conjugated with the MLA through the camera lens [1]. On the other hand, the pixelated sensor is conjugated with the camera lens (or, more specifically, with its exit pupil) through the microlenses. The images recorded by the sensor will be named *micro-images* here. In order to avoid overlapping between micro-images, the aperture angle of the camera lens must be equal to that of the microlenses.

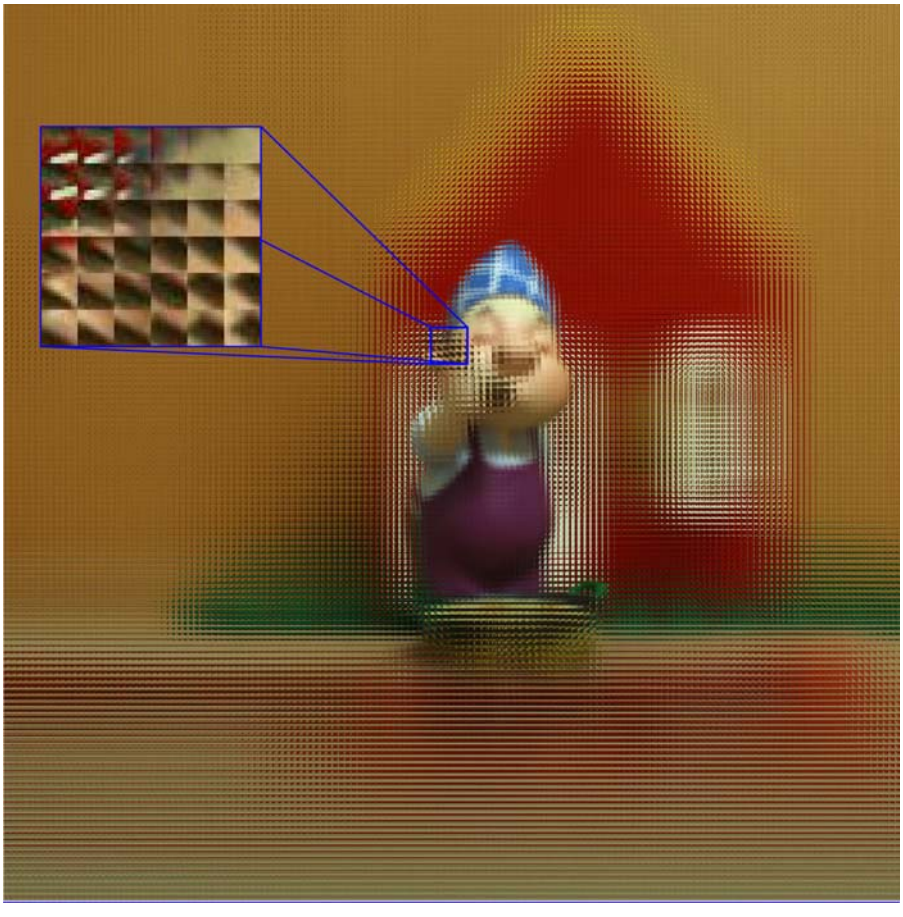

Figure 11.11 Micro-images calculated from the integral image. In the inset we show a subset of 6×6 micro-images

As shown in Fig. 11.12, the plenoptic camera does not directly capture the plenoptic field emitted by the 3D scene, but the one imaged by the camera lens. However, since there is a simple scaling relation between them, it is not difficult to calculate the plenoptic field in the object reference plane. Next, in Fig. 11.13 we depict the plenoptic field captured by the plenoptic camera in Fig. 11.12. Note that only the central pixel of the central microlens captures a ray with inclination $\theta = 0$, the rest of the central pixels capture rays whose inclination angle is proportional to the spatial coordinate of the center of the corresponding microlens. This is the reason for the sheared aspect of the captured plenoptic field.

Similar to that we explained in Section 11.4.1, the pixels in any vertical stack correspond to the micro-images. Here we can also compute sub-images, which are obtained by grouping pixels that have the same relative position in their respective micro-image (see the dotted envelope in Fig. 11.13). As we will see later, it is reasonable to name elemental images corresponding to the sub-images of the micro-images, and vice-versa.

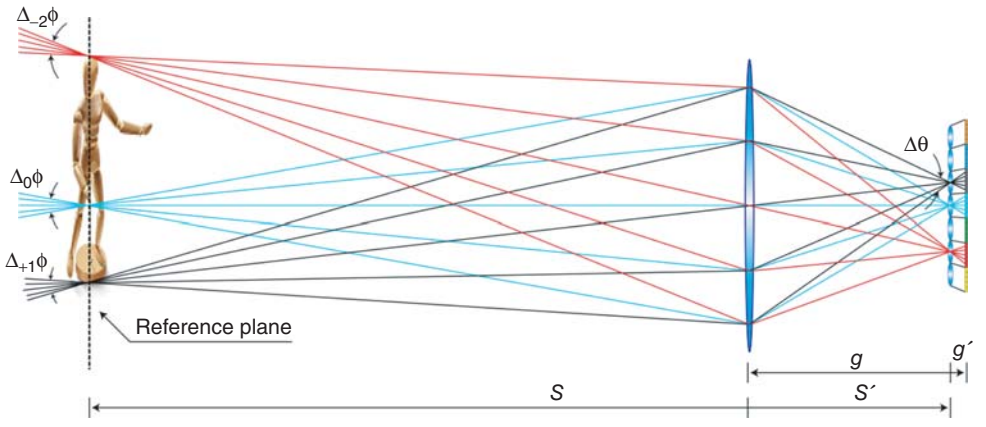

Figure 11.12 Scheme of the plenoptic camera

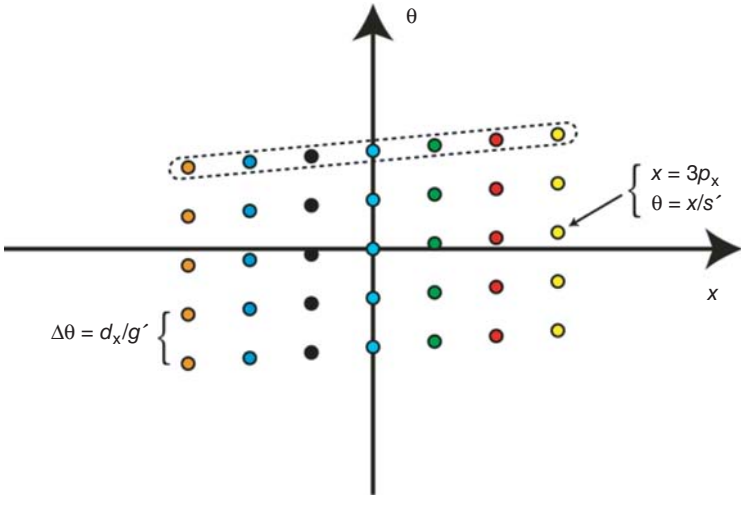

Figure 11.13 The sampled plenoptic field captured with the plenoptic camera of previous figure

Although there are already some commercial realizations of the plenoptic camera [60,61], we prepared our own plenoptic device in an open configuration in our laboratory. In Fig. 11.14 we show the experimental setup. A camera lens of $f = 100\,\text{mm}$ was used to conjugate the object reference plane with the MLA. The MLA was composed of a 94×59 lenslets of focal length $f_L = 0.93\,\text{mm}$ arranged in square grid of pitch $p_x = p_y = 0.222\,\text{mm}$ (APO-Q-P222-R0.93 model from AMUS). A digital camera with a macro objective 1:1 was used as the relay system that imaged the micro-images onto the sensor.

After the snapshot we obtained the plenoptic frame composed of 94×59 micro-images with 31×31 pixels each. The plenoptic frame is shown in Fig. 11.15. A pair of the computed sub-images is shown in Fig. 11.16.

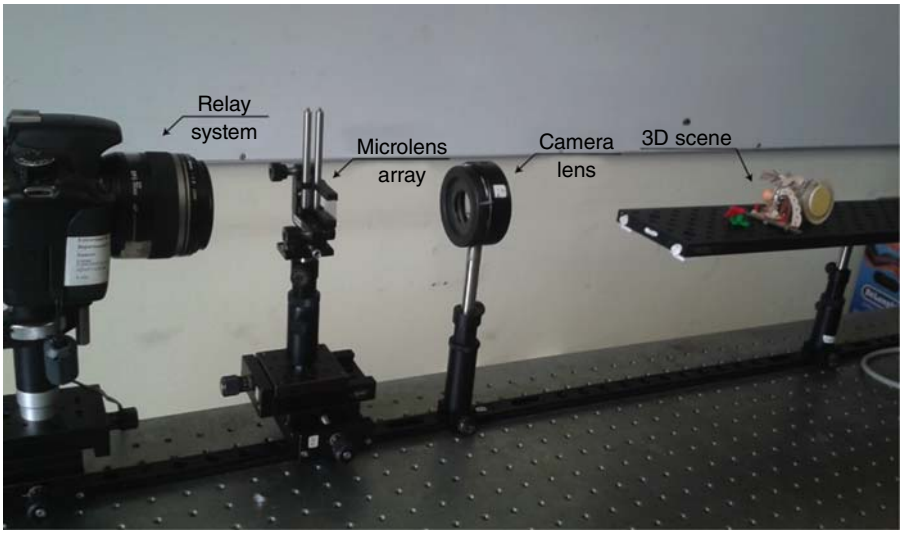

Figure 11.14 Experimental setup used for the capture of the plenoptic frame

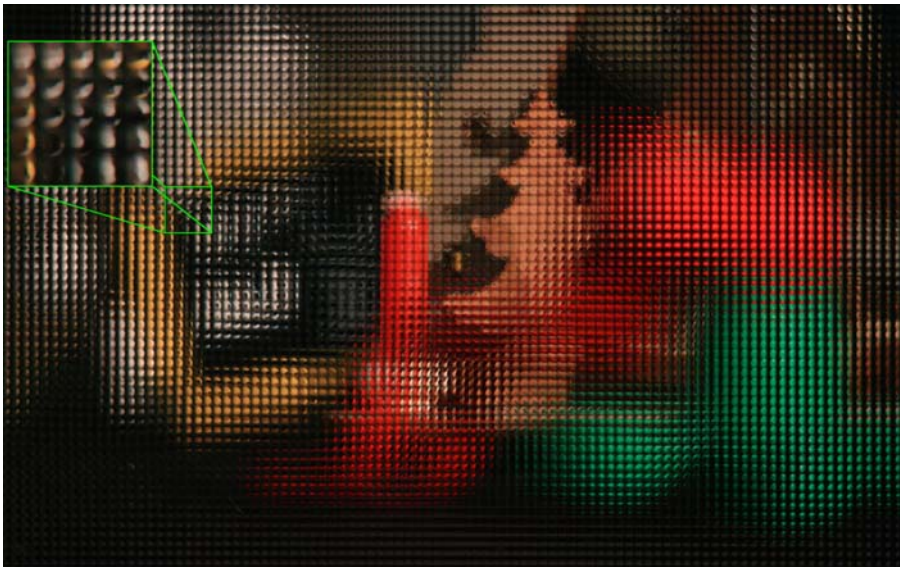

Figure 11.15 Captured plenoptic frame composed by 94×59 micro-images with 31×31 pixels each. In the inset we show a subset of 5×5 micro-images

Figure 11.16 Two of the subimages (also named *elemental images*) computed from the captured micro-images. From the plenoptic frame in Fig. 11.15 we could compute 31×31 elemental images composed of 94×59 pixels each. Note that any subimage observes the 3D scene from a different perspective

11.5 Walking in Plenoptic Space

As explained in Section 11.3, from the plenoptic function evaluated, or captured, in a given plenoptic reference plane, it is algebraically easy to calculate the plenoptic function in other planes, along with calculating the 2D pictures in such planes. To exemplify this, let us mark some specific planes in the plenoptic scheme depicted in Fig. 11.17(a) (Plate 18). To simplify the calculations, in this figure we have considered that the MLA is conjugated, through the camera lens, with infinity, so that $g = f$. Besides, since f is much larger than the focal length of the microlenses, the distance g' can be approximated by f_L.

Let us calculate first the plenoptic field at a plane (x_0, θ_0) placed in front of the MLA, at a distance t,

$$\begin{pmatrix} x_1 \\ \theta_1 \end{pmatrix} = T^{-1} \begin{pmatrix} x_0 \\ \theta_0 \end{pmatrix} = \begin{pmatrix} x_0 - t\theta_0 \\ \theta_0 \end{pmatrix}, \tag{11.7}$$

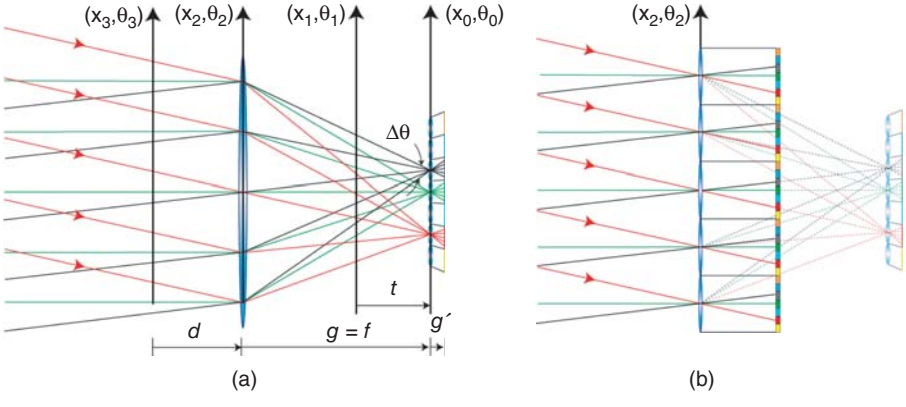

Figure 11.17 (Plate 18) (a) Scheme for the calculation of the plenoptic function in planes parallel to the MLA; (b) the plenoptic field as evaluated in the plane of the camera lens is equivalent to the one captured with an IP setup. *See plate section for the color version*

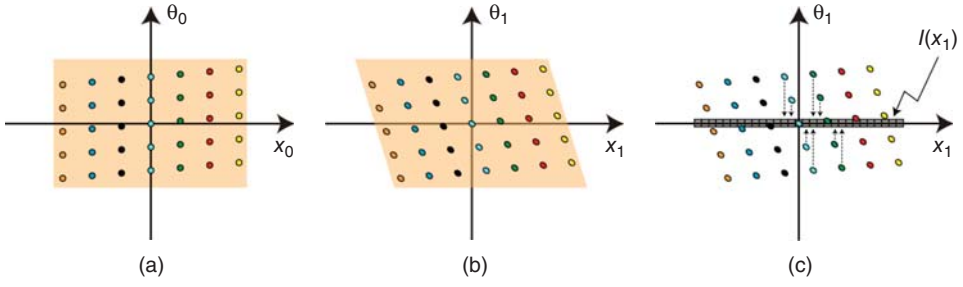

Figure 11.18 (a) Captured plenoptic field, (b) plenoptic field in the plane (x_1, θ_1), which is obtained after shearing the captured plenoptic function, and (c) irradiance distribution at the plane (x_1, θ_1), obtained after projecting the sheared plenoptic function

consequently,

$$L_1(x, \theta) = L_0(x - t\theta, \theta). \tag{11.8}$$

And therefore the picture in such plane can be calculated as

$$I_1(x) = \int L_0(x - t\theta, \theta)\, d\theta. \tag{11.9}$$

In Fig. 11.18 we illustrate this transformation. Note that Eqs (11.8) and (11.9) are valid for both positive and negative values of t, and therefore valid for calculating pictures in front or behind the MLA.

Now we calculate the plenoptic field in the plane of the camera lens (before the refraction),

$$\begin{pmatrix} x_2 \\ \theta_2 \end{pmatrix} = (T \cdot C)^{-1} \begin{pmatrix} x_0 \\ \theta_0 \end{pmatrix} = \begin{pmatrix} 1 & -f \\ 1/f & 0 \end{pmatrix} \begin{pmatrix} x_0 \\ \theta_0 \end{pmatrix} = \begin{pmatrix} x_0 - f\theta_0 \\ x_0/f \end{pmatrix}. \tag{11.10}$$

In Fig. 11.19 we illustrate this process.

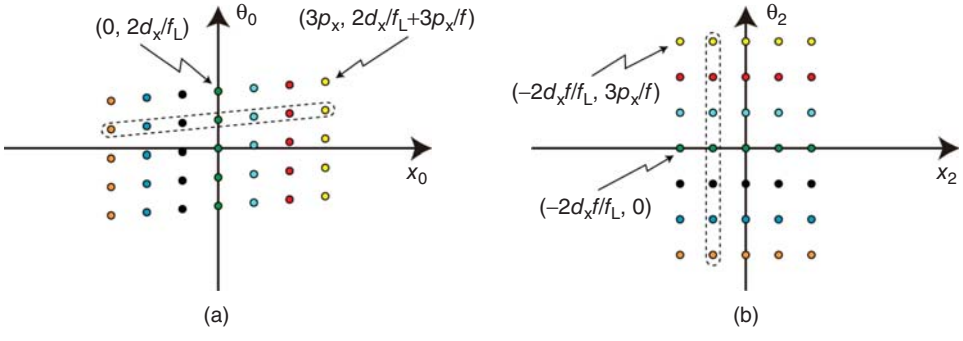

Figure 11.19 (a) Captured plenoptic field; (b) plenoptic field in the plane placed just before the refraction in the camera lens

As we can see from Eq. (11.10) and Fig. 11.19 (and have illustrated in Fig. 11.17(b)), the plenoptic field captured by the MLA placed at the back focal plane of the camera lens is nothing but a sheared and rotated version of the plenoptic field that could be captured by an adequate IP system placed at the camera-lens plane. A similar relation holds in the opposite direction; from the plenoptic field captured with an IP system, it is possible to calculate the plenoptic field captured by the proper plenoptic camera. The transposition relation of both plenoptic fields [15] can be useful for the calculation of elemental images from the micro-images captured with a plenoptic camera or vice versa. This property permits us, for example, to state that the micro-images calculated in Fig. 11.11 are similar to the micro-images captured directly with a proper plenoptic camera.

Finally, the plenoptic field at the plane (x_3, θ_3) can be calculated either from the plenoptic image or from the corresponding integral image,

$$\begin{pmatrix} x_3 \\ \theta_3 \end{pmatrix} = \begin{pmatrix} 1 & -d \\ 0 & 1 \end{pmatrix} \begin{pmatrix} x_2 \\ \theta_2 \end{pmatrix} = \begin{pmatrix} 1 - d/f & -f \\ 1/f & 0 \end{pmatrix} \begin{pmatrix} x_0 \\ \theta_0 \end{pmatrix}. \tag{11.11}$$

Therefore the picture in such plane can be calculated as

$$I_3(x) = \int L_2(x - \theta d, \theta)\, d\theta = \int L_0(x(1 - d/f) - f\theta, x/f)\, d\theta. \tag{11.12}$$

11.6 Reconstruction of Intensity Distribution in Different Depth Planes

As explained in Section 11.5, from the sampled version of the plenoptic field captured either with an IP setup or with a plenoptic camera, it is possible to calculate the irradiance distribution in different transverse sections of the original 3D scene. Although the integral image and the plenoptic image carry the same information, they are useful for different proposals. In particular, it is more convenient to use the integral image for implementing reconstruction algorithms, since it is composed of a low number of elemental images with a high number of pixels each.

The numerical reconstruction can be made by use of different algorithms. However, all are based on the same principle of shearing the plenoptic function and applying the Abel transform. This procedure can be visualized more intuitively, as shown in Fig. 11.20 (Plate 19), as projecting the pixels of any elemental image through a pinhole placed at the center of the corresponding microlens onto the corresponding reconstruction plane.

From the scheme, we can see that there is a univocal relation between the position of the reconstruction plane and the degree of overlapping between projected elemental images. Specifically, the degree of overlapping, M, is

$$M = \frac{z_R}{g} = \frac{N}{N - n}, \tag{11.13}$$

where N is the number of pixels per microlens and n is the number of pixels that overlap with the neighboring projected elemental image. It is apparent that the higher the degree of overlapping, the smaller the number of pixels of reconstructed images. To avoid unbalanced values of pixels of reconstructed images, the reconstructed pixels must be normalized, taking

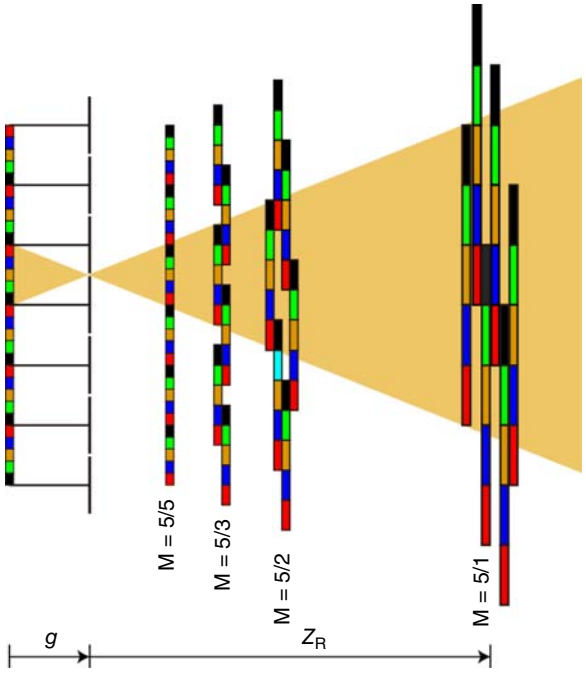

Figure 11.20 (Plate 19) Scheme of the conventional reconstruction algorithm. In this figure, the number of pixels per microlens is $N = 5$. *See plate section for the color version*

into account the number of projected pixels that contribute to any reconstructed pixel. In planes where the projected pixels do not match (i.e., in case of non-integer value of n) it is also possible to calculate the reconstruction. But the algorithm is slower, since it has to evaluate the percentage of contribution of any projected pixel to the pixels of the reconstructed images.

To show the power of reconstruction procedure, we have calculated, from the elemental images shown in Fig. 11.10, the irradiance distribution (i.e., the reconstructed picture) in some depth planes. The reconstructed pictures are shown in Fig. 11.21. Note that the resolution of the images is similar to the resolution of the elemental images [62]. The segmentation capacity, that is, the capacity of blurring images of out-of-focus planes, is determined by the number of elemental images and also by their parallax. In this experiment, the segmentation capacity is so high that the cook seems to disappear in the last reconstructed image.

As stated previously, the same reconstruction algorithm can be applied to the images obtained in the plenoptic experiment of Fig. 11.14. In this case the input for the algorithm is not the micro-images registered by the camera but the elemental images calculated after applying the transformation of Eq. (11.10). The reconstructed images are shown in Fig. 11.22. As in the previous case, the number of pixels of the elemental images (i.e., the number of micro-images) determines the resolution of reconstructed images. The number of elemental images (i.e., the number of pixels per micro-image) determines the segmentation capacity. These reconstructed images are poorer than the ones obtained here from the IP experiment. This is because the number of pixels in each elemental image, along with its parallax, is much lower.

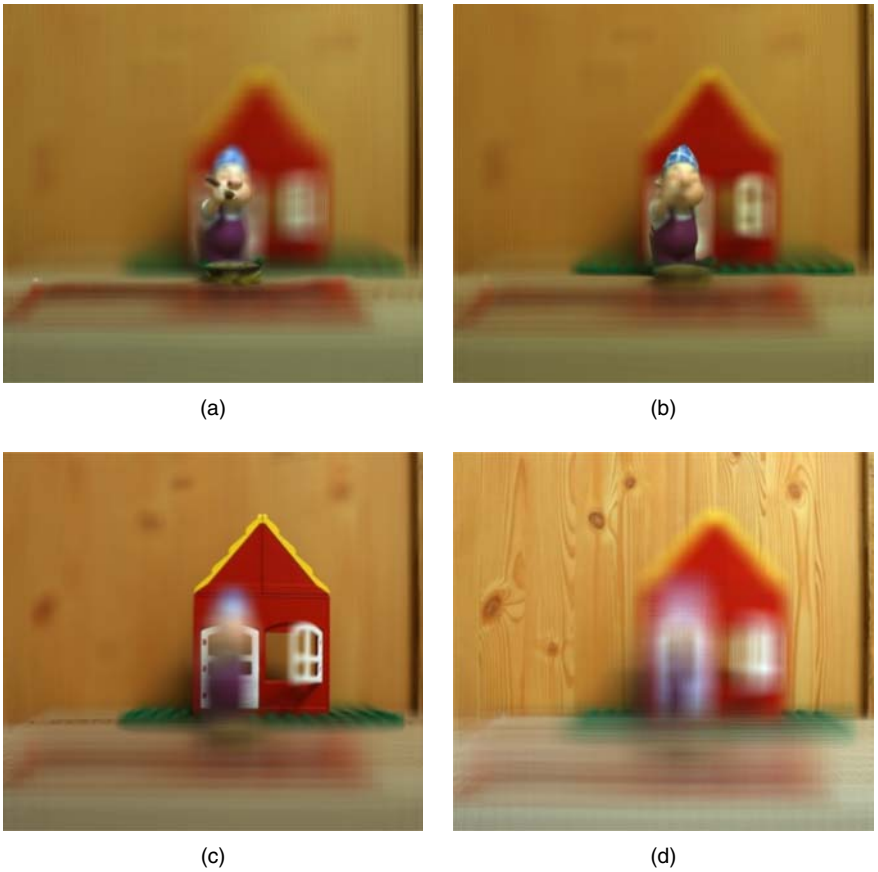

Figure 11.21 Reconstruction of the 3D scene in: (a) the plane of the hand; (b) the plane of the eyes; (c) the plane of the house; (d) the wooden panel

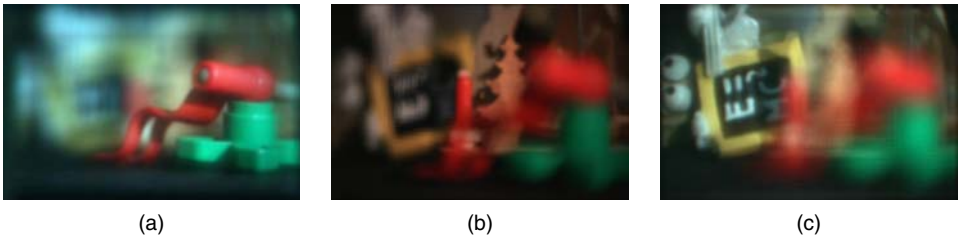

Figure 11.22 Reconstruction of the 3D scene in (a) the plane of the flag, (b) the plane of the fir, and (c) the plane of the chart

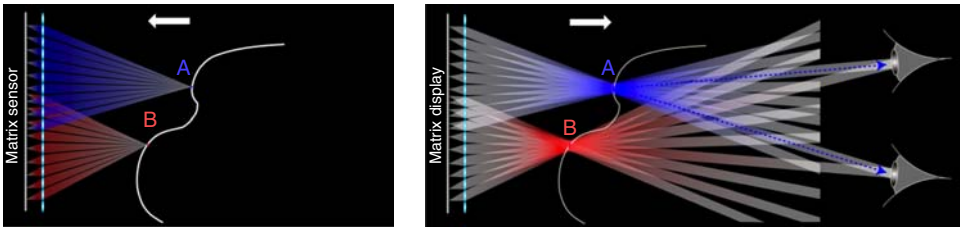

Figure 11.23 Scheme of capture and display process in integral photography. (a) In the capture stage any microlens stores different perspective information of the 3D scene. (b) In the display, any of the pixels in the panel can produce a light beam after passing through the corresponding microlens. The intersection of the light beams produces a light distribution that reconstructs the 3D scene

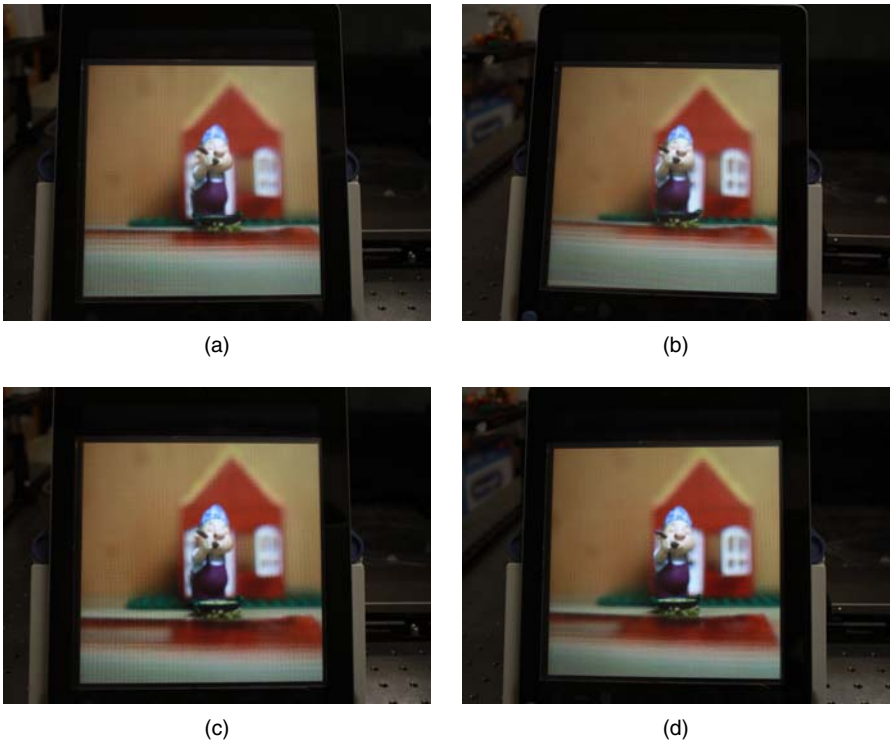

Figure 11.24 Four views of the 3D image displayed by the IP monitor after projecting on it the plenoptic frame as shown Fig. 11.11

11.7 Implementation of the Integral Imaging Display Device

When the integral (or the plenoptic) photography is acquired with the aim of projecting it onto an IP monitor, one should take into account the following facts. (1) The IP monitor is composed by a pixelated display (like a LCD or a LED display) and a MLA adjusted so that the display panel is at the front focal plane of the microlenses. (2) Since the resolution unit of an InI monitor is the pitch of the MLA [63], one should select a MLA with a high number of small microlenses. (3) Since the perspective resolution is determined by the number of pixels behind any microlens, one should arrange the display so that the number of pixels per microlens is about 12–16. (4) The images projected behind the MLA should be processed in a way that the monitor would project an orthoscopic 3D image. (5) The displayed 3D image should be centered at the display plane, so that some parts of the 3D image should be floating in front of the panel, and other parts should be behind it.

Next, in Fig. 11.23 we show a scheme of the display process in an InI monitor.

The easiest way of satisfying all the constraints listed previously is by projecting a plenoptic frame onto the display panel. As explained in previous sections, a plenoptic frame can be recorded directly with a plenoptic camera. Another solution is to record an IP with an array of digital cameras and later calculate the transposed plenoptic frame. Both, the IP and the plenoptic capture should take into account the parameters of the display. For example, we have prepared an IP monitor by using an iPad with retina display, consisting of 2048×1536 RGB pixels with width $\Delta_x = \Delta_y = 89.0\,\mu m$, and a MLA composed by lenses with $f_L = 3.0\,mm$ and pitch $p_x = p_y = 1.0\,mm$. Thus, the plenoptic frame should be composed by up to 186×140 micro-images with 11×11 pixels each.

The calculated plenoptic frame shown in Fig. 11.11 is precisely composed by micro-images with 11×11 pixels each. Thus, it is ready to be projected onto the display device. In Fig. 11.24 we show some views of the IP display. The horizontal and vertical parallax of the 3D image

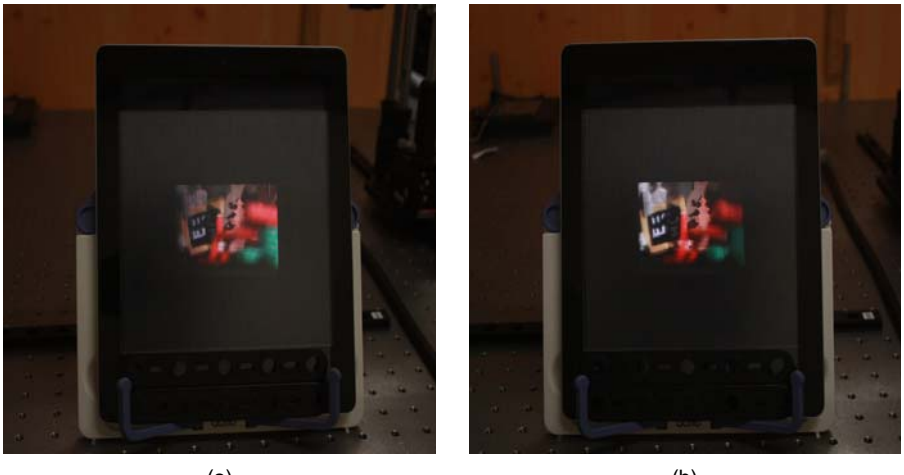

(a) (b)

Figure 11.25 Two views of the 3D image displayed by the IP monitor after projecting on it the plenoptic frame shown Fig. 11.15

displayed by the monitor can easily be seen. Although it is not possible to show it here, some parts of the displayed scene were floating out from the monitor and others into it. This was clearly seen by binocular observers.

In our second display experiment we projected onto the panel the plenoptic frame captured directly with the plenoptic camera, see Fig. 11.15. Note that although in Fig. 11.25 we show only the horizontal parallax, the displayed images also have vertical parallax. As in Section 11.6, the quality of this image is much poorer than that of the previous one. This is because the total number of pixels involved is much smaller.

Naturally there are some computational methods, not used here, that would permit to recalculate the plenoptic frame so that the number of micro-images and the number of pixels per microimage could be adapted to the parameters of the IP monitor [64,65].

11.8 Conclusion

The aim of this chapter is to expose integral photography; a technique that, although reported more than a century ago, has been recently revealed as the most effective method for the aim of projecting 3D pictures or movies to audiences or more than one person. We have explained the physics behind the IP concept and the relation to other realizations of the same concept. We have shown that there are mainly two different ways of implementing IP. In both cases, it is possible to apply computational reconstruction algorithms and also to implement IP monitors. Although the level of development of IP is currently high, a significant improvement in resolution, segmentation capacity, viewing angle, and development of new applications is expected in the next few years.

Acknowledgments

This work was funded by the Plan Nacional I+D+I (grant DPI2012-32994) Spain, and by the Generalitat Valenciana (grant PROMETEO2009-077).

References

[1] Ng R., *Digital light field photography*, Ph.D. Thesis (Stanford University, 2006).
[2] Wheatstone C., "Contributions to the physiology of vision", *Philosophical Transactions of the Royal Society of London* **4**, 76–77 (1837).
[3] Rollmann W., "Notiz zur Stereoskopie", *Ann. Phys.* **165**, 350–351 (1853).
[4] Kooi F. L. and A. Toet, "Visual comfort of binocular and 3D displays," *Displays* **25**, 99–108 (2004).
[5] Lippmann G., "Epreuves reversibles donnant la sensation du relief", *J. of Phys.* **7**, 821–825 (1908).
[6] Ives H. E., "Optical properties of a Lippman lenticulated sheet," *J. Opt. Soc. Am.* **21**, 171 (1931).
[7] Burckhardt C. B., "Optimum parameters and resolution limitation of integral photography," *J. Opt. Soc. Am. A* **58**, 71–74 (1968).
[8] Martínez-Corral M., H. Navarro, R. Martínez-Cuenca, G. Saavedra and B. Javidi, "Full parallax 3-D TV with programmable display parameters," *Opt. Phot. News* **22** (12), 50 (2011).
[9] Arai J., F. Okano, M. Kawakita, M. Okui, Y. Haino, M. Yoshimura, *et al*., "Integral three-dimensional television using a 33-megapixel imaging system," *J. Display Technol*. **6**, 422–430 (2010).

[10] Miura M., J. Arai, T. Mishina, M. Okui, and F. Okano, "Integral imaging system with enlarged horizontal viewing angle," *Proc. SPIE* **8384**, 83840o (2012).
[11] Davies N., M. McCormick, and L. Yang, "Three-dimensional imaging systems: a new development," *Appl. Opt.* **27**, 4520–4528 (1988).
[12] Adelson E. H. and J. Y. A. Wang, "Single lens stereo with plenoptic camera," *IEEE Trans. Pattern Anal. Mach. Intell*. **14**, 99–106 (1992).
[13] Georgiev T. and A Lumsdaine, "The focused plenoptic camera and rendering," *J. Elect. Imaging* **19**, 2 (2010).
[14] Ng R., M. Levoy, M. Brédif, G. Duval, M. Horowitz, and P. Hanrahan, "Light field photography with a hand-held plenoptic camera", *Tech. Rep. CSTR 2*, (2005).
[15] Levoy M., R. Ng, A. Adams, M. Footer, and M. Horowitz, "Light field microscopy," *ACM SIGGRAPH* 924–934 (2006).
[16] Navarro H., J. C. Barreiro, G. Saavedra, M. Martínez-Corral, and B. Javidi, "High-resolution far-field integral-imaging camera by double snapshot," *Opt. Express* **20**, 890–895 (2012).
[17] Okano F., J. Arai, H. Hoshino, and I. Yuyama, "Three-dimensional video system based on integral photography," *Opt. Eng.* **38**, 1072–1077 (1999).
[18] Park J.-H., K. Hong, and B. Lee, "Recent progress in three-dimensional information processing based on integral imaging," *Appl. Opt.* **48**, H77–H94 (2009).
[19] Arai J., M. Kawakita, T. Yamashita, H. Sasaki, M. Miura, H. Hiura, *et al*. "Integral three-dimensional television with video system using pixel-offset method," *Opt. Express* **21**, 3474–3485 (2013).
[20] Javidi B. and J.-S. Jang, "Improved resolution 3D TV, video, and imaging using moving microoptics array lens techniques and systems (MALTS)," *Proc. SPIE* **4902**, 1–12 (2002).
[21] Lim Y.-T., J.-H. Park, K.-C. Kwon, and N. Kim, "Resolution-enhanced integral imaging microscopy that uses lens array shifting," *Opt. Express* **17**, 19253–19263 (2009).
[22] Navarro H., R. Martínez-Cuenca, A. Molina-Martín, M. Martínez-Corral, G. Saavedra, and B. Javidi, "Method to remedy image degradations due to facet braiding in 3D integral imaging monitors," *J. Disp. Technol*. **6**, 404–411 (2010).
[23] Lee B., S. Jung, and J.-H. Park, "Viewing-angle-enhanced integral imaging by lens switching," *Opt. Lett.* **27**, 818–820 (2002).
[24] Choi H., S.-W. Min, S. Jung, J.-H. Park, and B. Lee, "Multiple-viewing-zone integral imaging using a dynamic barrier array for three-dimensional displays," *Opt. Express* **11**, 927–932 (2003).
[25] Martínez-Cuenca R., H. Navarro, G. Saavedra, B. Javidi, M. Martínez-Corral, "Enhanced viewing-angle integral imaging by multiple-axis telecentric relay system," *Opt. Express* **15**, 16255–16260 (2007).
[26] Zhang L., Y. Yang, X. Zhao, Z. Fang, and X. Yuan, "Enhancement of depth-of-field in a direct projection-type integral imaging system by a negative lens array," *Opt. Express* **20**, 26021–26026 (2012).
[27] Bagheri S., Z. Kavehvash, K. Mehrany, and B. Javidi, "A fast optimization method for extension of depth-of-field in three-dimensional task-specific imaging systems," *J. Display Technol*. **6**, 412–421 (2010).
[28] Tolosa A., R. Martínez-Cuenca, A. Pons, G. Saavedra, M. Martínez-Corral, and B. Javidi, "Optical implementation of micro-zoom arrays for parallel focusing in integral imaging," *J. Opt. Soc. Am. A* **27**, 495–500 (2010).
[29] Xiao X., B. Javidi, M. Martínez-Corral, and A. Stern, "Advances in three-dimensional integral imaging: sensing, display, and applications," *Appl. Opt.* **52**, 546–560 (2013).
[30] McMillan L. and G. Bishop, "Plenoptic modeling: an image-based rendering system," *Proc. ACM SIGGRAPH Conf. on Comp. Graphics* 39–46 (1995).
[31] Chai J.-X., X. Tong, S.-C. Chan, and H.-Y. Shum, "Plenoptic sampling," *Proc. ACM SIGGRAPH Conf. on Comp. Graphics* 307–318 (2000).

[32] Kishk S. and B. Javidi, "Improved resolution 3D object sensing and recognition using time multiplexed computational integral imaging," *Opt. Express* **11**, 3528–3541 (2003).
[33] Hong S. H., J. S. Jang, and B. Javidi, "Three-dimensional volumetric object reconstruction using computational integral imaging," *Opt. Express* **1**, 483–491 (2004).
[34] Levoy M., "Light fields and computational imaging", *IEEE Computer* **39**, 46–55 (2006).
[35] Cho M. and B. Javidi, "Computational reconstruction of three-dimensional integral imaging by rearrangement of elemental image pixels," *J. Disp. Technol*. **5**, 61–65 (2009).
[36] Navarro H., E. Sánchez-Ortiga, G. Saavedra, A. Llavador, A. Dorado, M. Martínez-Corral, and B. Javidi, "Non-homogeneity of lateral resolution in integral imaging," *J. Display Technol*. **9**, 37–43 (2013).
[37] Park J.-H., S. Jung, H. Choi, Y. Kim, and B. Lee, "Depth extraction by use of a rectangular lens array and one-dimensional elemental image modification," *Appl. Opt.* **43**, 4882–4895 (2004).
[38] DaneshPanah M. and B. Javidi, "Profilometry and optical slicing by passive three-dimensional imaging," *Opt. Lett*. **34**, 1105–1107 (2009).
[39] Saavedra G., R. Martínez-Cuenca, M. Martínez-Corral, H. Navarro, M. Daneshpanah and B. Javidi, "Digital slicing of 3D scenes by Fourier filtering of integral images," *Opt. Express* **16**, 17154–17160 (2008).
[40] Park J. H. and K. M. Jeong, "Frequency domain depth filtering of integral imaging," *Opt. Express* **19**, 18729–18741 (2011).
[41] Park J.-H., J. Kim, and B. Lee, "Three-dimensional optical correlator using a sub-image array," *Opt. Express* **13**, 5116–5126 (2005).
[42] Matoba O., E. Tajahuerce, and B. Javidi, "Real-time three-dimensional object recognition with multiple perspectives imaging," *Appl. Opt.* **40**, 3318–3325 (2001).
[43] Cho M. and B. Javidi, "Three-dimensional visualization of objects in turbid water using integral imaging," *J. Disp. Technol*. **6**, 544–547 (2010a).
[44] Hong S. H. and B. Javidi, "Distortion-tolerant 3D recognition of occluded objects using computational integral imaging," *Opt. Express* **14**, 12085–12095 (2006).
[45] Cho M. and B. Javidi, "Three-dimensional visualization of objects in turbid water using integral imaging," *J. Disp. Technol*. **6**, 544–547 (2010b).
[46] DaneshPanah M., B. Javidi, and E. A. Watson, "Three dimensional object recognition with photon counting imagery in the presence of noise," *Opt. Express* **18**, 26450–26460 (2010).
[47] Zhao Y., X. Xiao, M. Cho, and B. Javidi, "Tracking of multiple objects in unknown background using Bayesian estimation in 3D space," *J. Opt. Soc. Am. A* **28**, 1935–1940 (2011).
[48] Lynch K., T. Fahringer, and B. Thurow, "Three-dimensional particle image velocimetry using a plenoptic camera," *AIAA*–**1056**, 1–14 (2012).
[49] Xiao X., B. Javidi, G. Saavedra, M. Eismann, and M. Martinez-Corral, "Three-dimensional polarimetric computational integral imaging," *Opt. Express* **20**, 15481–15488 (2012).
[50] Latorre-Carmona P., E. Sánchez-Ortiga, X. Xiao, F. Pla, M. Martínez-Corral, H. Navarro, G. Saavedra, and B. Javidi," Multispectral integral imaging acquisition and processing using a monochrome camera and a liquid crystal tunable filter," *Opt. Express* **20**, 25960–25969 (2012).
[51] Jang J.-S. and B. Javidi, "Three-dimensional integral imaging of micro-objects," *Opt. Lett*. **29**, 1230–1232 (2003).
[52] Levoy M., Z. Zhang, and I. McDowall, "Recording and controlling the 4D light field in a microscope using microlens arrays," *J. Micros*. **235**, 144–162 (2009).
[53] Lim Y.-T., J.-H. Park, K.-C. Kwon, and N. Kim, "Resolution-enhanced integral imaging microscopy that uses lens array shifting," *Opt. Express* **17**, 19253–19263 (2009).
[54] Rodríguez-Ramos L. F., I. Montilla, J. J. Fernández-Valdivia, J. L. Trujillo-Sevilla, and J. M. Rodríguez-Ramos, "Concepts, laboratory and telescope test results of the plenoptic camera as a wavefront sensor," *Proc. SPIE* **8447**, 844745 (2012).
[55] Saleh B. E. A. and M. C. Teich, *Fundamentals of Photonics*. Chichester: John Wiley & Sons, Ltd (1991).

[56] Gorenflo R. and S. Vessella, *Abel Integral Equations: Analysis and Applications*, Lect. Notes Math., Vol. **1461**, Berlin, Heidelberg, New York: Springer (1991).
[57] Tanida J., K. Yamada, S. Miyatake, K. Ishida, T. Morinoto, N. Kondou, *et al*., "Thin observation module my bound optics (TOMBO): concept and experimental verification," *Appl. Opt.* **40**, 1806–1813 (2001).
[58] ProFUSION25. 5×5 Digital Camera Array. Website, available at: www.ptgrey.com/products/profusion25/ProFUSION_25_datasheet.pdf (accessed December 6, 2013).
[59] Jang J. S. and B. Javidi, "Three-dimensional synthetic aperture integral imaging," *Opt. Lett*. **27**, 1144–1146 (2002).
[60] 3D lightfield camera. Website, available at: www.raytrix.de/ (accessed December 5, 2013).
[61] Lightfield based commercial digital still camera. Website, available at: www.lytro.com (accessed December 5, 2013).
[62] Kavehvash Z., M. Martinez-Corral, K. Mehrany, S. Bagheri, G. Saavedra, and H. Navarro, "Three-dimensional resolvability in an integral imaging system," *J. Opt. Soc. Am. A* **29**, 525–530 (2012).
[63] Martínez-Cuenca R., G. Saavedra, M. Martínez-Corral, and B. Javidi, "Progresses in 3-D multiperspective display by integral imaging," *Proc. IEEE* **97**, 1067–1077 (2009).
[64] Navarro H., R. Martínez-Cuenca, G. Saavedra, M. Martínez-Corral, and B. Javidi, "3D integral imaging display by smart pseudoscopic-to-orthoscopic conversion," *Opt. Express* **18**, 25573–25583 (2010).
[65] Jung J.-H., J. Kim, and B. Lee, "Solution of pseudoscopic problem in integral imaging for real-time processing," *Opt. Lett.* **38**, 76–78 (2013).